

Model Predictive Control of Energy Storage including Uncertain Forecasts

Michèle Arnold, Göran Andersson

ETH Zurich

Zurich, Switzerland

arnold@eeh.ee.ethz.ch, andersson@eeh.ee.ethz.ch

Abstract - The intermittency of renewable energy sources, e.g. wind or solar, as well as forecast uncertainties in load, price and renewable infeed profiles call for storage solutions and appropriate control strategies. For the investigations in this paper the energy hub modeling framework is used, which takes into account multiple energy carriers, distributed generation, energy storage systems and renewable energy sources. This paper focuses on the value of energy storage devices when operating them in combination with intermittent infeed from renewable energy sources. Since forecasts never are perfect, a model predictive control (MPC) strategy is used for keeping the consequences of forecast uncertainties at acceptable levels. Instead of compensating forecast uncertainties with fast acting backup generators or balancing energy, the imbalances can be compensated by means of storage devices, placed close to locations where uncertainties arise. Monte-Carlo simulations show that major part of the disturbances can be compensated by means of storage devices without increasing system operation costs significantly. In cases where storage devices are not sufficient, generator settings are changed from day-ahead schedule, representing additional balancing costs.

Keywords - Power system optimization, model predictive control, energy storage, forecast errors, multi-carrier energy systems

1 Introduction

THE increasing penetration of distributed generation (DG) technologies, such as photovoltaics, wind turbines, micro combined heat and power plants (μ CHP), biomass-fired plants and others, leads to new challenges in operation of power systems. Moreover, the intermittency of local renewable energy sources (RES), e.g., wind and solar power, as well as the uncertainties in their predicted available power output, create the need for storage solutions and appropriate control strategies. Beyond that, forecast errors in price and load profiles further complicate the establishment of the generation-load balance. So far, imbalances between production and load are compensated by the grid and fast acting backup generators such as gas turbines or hydro storage power plants. However, due to the on-going increase in intermittent sources, day-ahead planning becomes more demanding. Grid operators often have to pay high penalties due to re-scheduling because they cannot meet their projected production pattern due to inaccurate forecasts. Furthermore, an increasing number of backup generation units is needed, running on reduced power or even on idle, to quickly react to output changes of intermittent sources. Instead of compensating

forecast uncertainties with fast acting backup generators or balancing energy, as it is often done in current practice, the imbalances can also be compensated by means of storage devices, placed close to locations where uncertainties arise. In [1], the benefits of using storage for providing balancing services for electricity generation systems with high wind penetration are evaluated. The authors show that compared with other balancing solutions storage devices save fuel costs and reduce CO₂ emissions. In [2], storage devices are used to balance power fluctuations of non-dispatchable generators in order to feed power into the network according to an hourly pre-determined constant profile.

For taking into account distributed generation, storage devices and renewable energy sources, the energy hub modeling framework [3] is used. Energy hubs are primarily used to describe systems comprising multiple energy carriers. Increasingly, energy supply is no longer based only on electricity networks, but other energy carrier networks, such as natural gas or heating networks, have to be taken into account as well. These multi-carrier energy systems are considered to consist of a number of interconnected energy hubs, which represent the interface between consumers and power supply infrastructures of different energy systems.

A two-level control scheme is applied, which is divided into day-ahead planning and on-line dispatch. The on-line procedure adapts pre-defined generation settings (determined by the day-ahead planner) to profile changes appearing within the day. An appropriate on-line control procedure wherewith system dynamics and forecast uncertainties can be taken into account is Model Predictive Control (MPC). By using a predictive approach, fluctuations within energy prices, load profiles and input profiles from renewable energy sources can be handled in an appropriate way. Applying MPC, storage devices are operated in a cost-efficient way, wherewith most forecast uncertainties are balanced by means of storage devices such that adjustments of backup generators or penalties for balancing energy are reduced.

The remainder of this paper is organized as follows. Section 2 describes the modeling framework of storage devices, energy hubs and energy transmission systems. In Section 3, the MPC control approach is presented, followed by its application to the system, Section 4. Simulation results, applying the proposed control strategy to a two-hub system are presented in Section 5. Section 6 concludes this paper and outlines directions for future research.

2 Modeling Framework

In this section, the mathematical model of multi-carrier energy systems is presented. Firstly, the storage model is described. Next, the energy hub which couples both systems is formalized. Finally, the transmission systems are described. All equations are defined for time step k as we consider the optimal operation over multiple time steps. A discrete time step k corresponds to the continuous time kT , where T is one hour.

2.1 Energy Storage

In the considered system setup, hot water and battery storage devices are implemented. For both storage devices the same models are used, but with different parameters. A storage device is modeled as ideal storage in combination with a storage interface. The power exchange $M_\alpha(k)$ is defined as the difference between stored amount of energy $E_\alpha(k)$ at two consecutive time steps, plus some standby energy losses $\dot{E}_\alpha^{\text{stb}}$, which must be covered at each time period ($\dot{E}_\alpha^{\text{stb}} \geq 0$):

$$\begin{aligned} M_\alpha(k) &= \frac{\dot{E}_\alpha}{e_\alpha} = \frac{1}{e_\alpha} \frac{dE_\alpha}{dt} \approx \frac{1}{e_\alpha} \frac{\Delta E_\alpha}{\Delta t} \\ &= \frac{1}{e_\alpha} \left(\frac{E_\alpha(k) - E_\alpha(k-1)}{\Delta t} + \dot{E}_\alpha^{\text{stb}} \right). \end{aligned} \quad (1)$$

The parameters e_α^+ , e_α^- are the charging and discharging efficiencies of the storage device, respectively. The subscript α stands for both storage mediums, heat and electricity.

The stored energy $E_\alpha(k)$ and the power exchange $M_\alpha(k)$ have to remain within limits, resulting in the following constraints for the storage device:

$$M_{\alpha,\min}(k) < M_\alpha(k) < M_{\alpha,\max}(k) \quad (2)$$

$$E_{\alpha,\min}(k) - \varepsilon(k) < E_\alpha(k) < E_{\alpha,\max}(k) + \varepsilon(k) \quad (3)$$

$$\varepsilon(k) \geq 0 \quad (4)$$

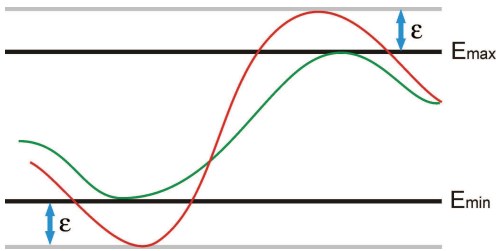


Figure 1: Illustration of soft constraints: Storage capacity modeled without soft constraints (green curve) and with soft constraints (red curve).

In order to avoid system infeasibility in cases of high forecast errors, storage capacity limits are modeled as soft constraints. Therewith, storage devices are allowed to shortly violate their optimal operation limits (Fig. 1). This is reasonable since storage devices always have some reserve capacity in reality. When the optimal operation interval is violated, additional costs arise by adding the slack variables, ε , with an appropriate weighting factor to the objective function (Sect. 4.3). Doing so, it is guaranteed, that the optimal operation limits are only violated if

the secure system operation is endangered. Nevertheless, storage capacities have to respect some hard limits, which represent the physical limits of the storage.

2.2 Energy Hub

Energy hubs formalize the modeling of a system consisting of multiple energy carriers. By means of the energy hub concept, storage of different forms of energy and conversion between them can be formulated [3]. Figure 2 shows an illustrative example for an energy hub, which consumes/delivers electricity P_e^H and consumes natural gas P_g^H at the input and supplies energy to electric L_e and heat loads L_h . The hub contains a μ CHP and a furnace for energy conversion and a heat and a electric storage for energy storage. The electricity produced using the μ CHP can either be used for load supply, for filling up the electric storage or can be, depending on price and load profiles, fed back to the grid. The heat produced, by both μ CHP and furnace, is either used to supply the heat load or to fill up the heat storage. If the produced heat is not sufficient to cover the heat demand, the storage is used for support. The coupling provided by the μ CHP device increases the redundancy in supply and offers the opportunity of optimizing the energy supply, e.g., supplying the electric load via μ CHP which is particularly lucrative at high electricity import prices.

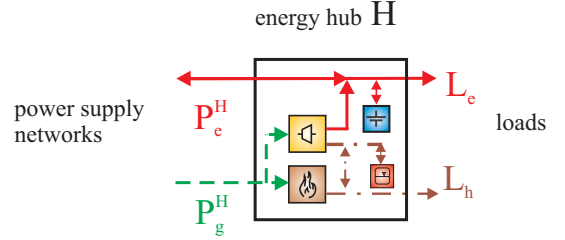


Figure 2: Example of an energy hub containing μ CHP device, furnace, thermal and electric storage. Hub is connected to electricity and natural gas power supply networks and supplies electric and thermal loads.

For the energy hub depicted in Fig. 2, the outputs $\mathbf{L}(k) + \mathbf{M}(k)$ and inputs $\mathbf{P}(k)$ at time step k are correlated as follows:

$$\underbrace{\begin{bmatrix} L_e(k) + M_e(k) \\ L_h(k) + M_h(k) \end{bmatrix}}_{\mathbf{L}(k) + \mathbf{M}(k)} = \underbrace{\begin{bmatrix} 1 & \nu(k)\eta_{ge}^{\text{CHP}} \\ 0 & \nu(k)\eta_{gh}^{\text{CHP}} + (1 - \nu(k))\eta_{gh}^{\text{F}} \end{bmatrix}}_{\mathbf{C}(k)} \underbrace{\begin{bmatrix} P_e^H(k) \\ P_g^H(k) \end{bmatrix}}_{\mathbf{P}(k)}, \quad (5)$$

where $\mathbf{C}(k)$ describes the coupling and conversion between the input and output carriers. The converter devices are modeled as coupling factors, composed of the converter's steady-state energy efficiency and a dispatch factor. The parameters η_{ge}^{CHP} , η_{gh}^{CHP} denote the gas-electric and gas-heat efficiencies of the μ CHP and η_{gh}^{F} defines the efficiency of the furnace. The dispatch factor $\nu(k)$ ($0 \leq \nu(k) \leq 1$) determines how the gas is divided between the μ CHP and the furnace. The energy storage devices are modeled as illustrated above. As the dispatch

factor $\nu(k)$ is a control variable, different input vectors can be found to fulfill the output requirements. This reflects the degrees of freedom in supply which are used for optimization.

2.3 Energy Transmission System

Both transmission systems, electricity and gas pipeline networks, are modeled by nodal power flow and nodal volume flow equations, respectively. Electric power flows are formulated as nodal power balances of complex power using line equations according to [4], [5]. Gas volume flows are formulated as nodal volume flow balances using line and compressor equations according to [5]. A gas pipeline is composed of a compressor element, with pressure amplification p_{inc} , and a pipeline element. A more detailed description of the energy transmission network can be found in [5].

3 Control Strategy

A controller has to be implemented that determines operational system set-points in such a way that overall operation costs are minimized while satisfying all system constraints. Since storage dynamics have to be coped with, a multi-time step optimization is required. Furthermore, forecast uncertainties arise which can be handled by applying a receding horizon control strategy. Model predictive control (MPC) provides an appropriate control approach for taking into account both, system dynamics and forecast uncertainties. As illustrated in Fig. 3, the whole control procedure is carried out at two levels.

Day-ahead planning: Firstly, a day-ahead planning is performed. Based on bids and contracts, TSOs define settings of generation units for the next 24 hours. Thereby, best available forecasts of load profiles and renewable infeed profiles are used. The pre-scheduled generation settings are further referred to as $\mathbf{P}^{G,Sched}$.

On-line dispatch: Secondly, an on-line control procedure adapts the pre-defined generation settings to profile changes occurring during the day. MPC is chosen to perform this on-line control. The MPC controller works with updated forecast profiles and determines generation settings $\mathbf{P}^{G,MPC}$ close to $\mathbf{P}^{G,Sched}$ to avoid expensive balancing energy.

Day-ahead Planning

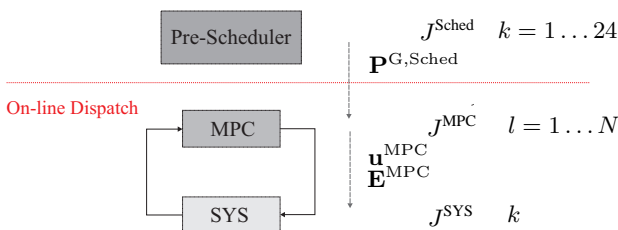


Figure 3: Illustration of two-level control strategy, involving tree optimization problems: day-ahead planning (Pre-Scheduler), on-line dispatch (MPC) and application to the system (SYS).

3.1 Model Predictive Control

Model Predictive Control (MPC) [6] is a widely used control strategy. It is an optimization based control strategy which uses an internal model to find those control inputs that yield the best predicted behavior of the system over a prediction horizon with length N . It operates in a receding horizon fashion, i.e. at every time step updated system measurements and forecasts are used to predict the future behavior of the system. Applying MPC, the controller is able to anticipate future events and changes, such as increasing or decreasing energy prices. Furthermore, consequences of forecast uncertainties are minimized thanks to the operation in a receding horizon mode.

Figure 3 illustrates the principle of MPC, showing the interactions between system and controller. Based on the current system state $\mathbf{x}(k)$, the controller determines control inputs $\tilde{\mathbf{u}}(k) = [\mathbf{u}^T(k), \dots, \mathbf{u}^T(k+N-1)]^T$, that yield the best predicted performance of the system over the next N time steps. The control variables for the current time step $\mathbf{u}(k)$ are applied to the system, which then proceeds to a new system state $\mathbf{x}(k+1)$. Now, the whole procedure starts again with updated system measurements and new forecasts.

4 Application to System

The control strategy explained above is now applied to multi-carrier energy systems. Variables, objectives and constraints are formulated for the system depicted below.

4.1 System setup

The multi-carrier energy system consists of an integrated electricity and natural gas system, interconnecting two energy hubs to the supply grid (Fig. 4). The hubs and their loads represent an aggregation of households and are structured as described in Sect. 2.2. Within the residential areas, i.e. energy hubs, renewable energy sources, such as photovoltaic (PV) or wind installations are available, modeled as infeeds R_1 and R_2 . The supply grid is modeled by electric generator G_1 and gas network N . The electricity system is modeled on three voltage levels. The households are connected to the low voltage level, e.g. 400 V. On the medium voltage level (e.g. 16 kV), local generation units, such as waste incineration plants or biomass-fired plants are placed. Generator G_1 , located at bus 4, e.g. 60 kV, represents the grid, modeled as infinite bus and represents the slack node of the electricity system. The gas pipeline network is modeled on a single pressure level, where N supplies all gas demands. The compressors C_{12} , C_{13} enable the gas flow to the hubs. For further information about the system parameters, refer to [5].

This system setup takes into account the increased penetration of distributed generation (μ CHP and local generators) and of renewable infeed (wind and PV). Each household within the hub decides autonomously when to produce electricity locally via μ CHP, when to store energy and to feed it back to the grid at a later instant, or when to consume energy from higher network levels.

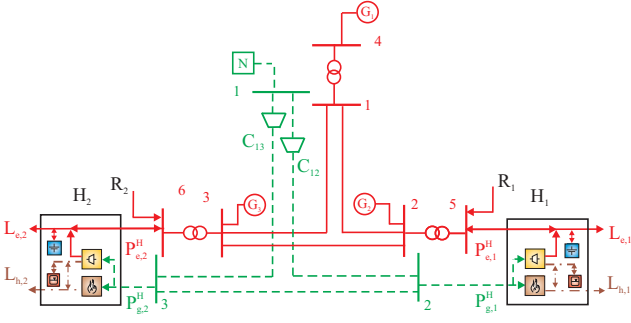


Figure 4: System setup of two energy hubs connected to the supply grid. Active power is provided by generators G_1 , G_2 , G_3 , natural gas by the adjacent natural gas network N . Both hubs have renewable infeeds R_1 and R_2 .

4.2 Variables

For modeling the combined electricity and gas network, all system variables are collected in the following three vectors:

control vector $\mathbf{u}(k)$:

$$\mathbf{u}(k) = [(\mathbf{P}_e^G)^T(k) \quad P_g^G(k) \quad \boldsymbol{\nu}_g^T(k)]^T, \quad (6)$$

where

- $\mathbf{P}_e^G(k)$ denotes the active power generation of all generators,
- $P_g^G(k)$ defines the natural gas import and
- $\boldsymbol{\nu}_g(k)$ describes the dispatch factors at the gas input junctions.

dynamic $\mathbf{x}(k)$ and static $\mathbf{z}(k)$ state vectors:

$$\mathbf{x}(k) = [\mathbf{E}_h(k), \mathbf{E}_e(k)]^T, \quad (7)$$

$$\mathbf{z}(k) = [\mathbf{V}^T(k) \quad \boldsymbol{\theta}^T(k) \quad \mathbf{p}^T(k) \quad \mathbf{p}_{\text{inc}}^T(k) \quad (\mathbf{P}_e^H)^T(k) \quad (\mathbf{P}_g^H)^T(k)]^T, \quad (8)$$

where

- $\mathbf{V}(k)$ and $\boldsymbol{\theta}(k)$ denote the voltage magnitudes and angles of all electric buses, respectively,
- $\mathbf{p}(k)$ denotes the nodal pressures of all gas buses,
- $\mathbf{p}_{\text{inc}}(k)$ denotes the pressure amplification of both compressors,
- $\mathbf{P}_e^H(k)$ and $\mathbf{P}_g^H(k)$ denote the electric and gas inputs of the hubs, respectively, and
- $\mathbf{E}_h(k)$ and $\mathbf{E}_e(k)$ denote the energy contents of the heat and electric storage devices, respectively.

The input profiles from renewable energy sources are assumed to be non-controllable. Further studies could consider renewable infeed as control variable, where the power can be curtailed if only part of it should be fed into the system. Here, we use bus 4, which is the slack node of the system, to overcome this problem. If e.g. wind power exceeds system demand including storage capacities, the

exceeding power is fed back to the grid. Therewith, storages and their maximum needed capacities are released. Also, load profiles of electricity and heat demand are considered to be given. Further studies could model these as control variables as well, to incorporate load management schemes.

4.3 Objective and Constraints

As mentioned above, the control procedure is carried out on two levels. This results in three optimization problems: day-ahead planning, on-line dispatch performed by the MPC controller, and application to the system.

Day-ahead planning: Firstly, the pre-scheduler runs a day-ahead optimization which is a multi-period optimization performed over 24 hours. The objective of the day-ahead planner is:

$$J^{\text{Sched}} = \sum_{k=1}^{24} \sum_{i_G=1}^3 [q_{i_G}^G(k) (P_{e,i_G}^G(k))^2] \quad (9)$$

$$+ q^N(k) P_g^G(k)] \quad (10)$$

$$+ c_\varepsilon \sum_{k=1}^{24} \sum_{i_E \in \Omega_E} (\varepsilon_{i_E}(k))^2 \quad (11)$$

where (9) corresponds to the overall costs of electricity and (10) of natural gas consumption ($q_{i_G}^G$ and q^N define time varying prices (Fig. 5)). The last term (11) represents penalties for all storage devices i_E in Ω_E when they are passing their optimal operation limits. The day-ahead schedule of the generation units is stored in $\mathbf{P}^{G,\text{Sched}} = [P_{e,i_G}^{G,\text{Sched}} \quad P_{g,i_G}^{G,\text{Sched}}]$.

MPC controller: The MPC controller again minimizes overall operation costs, but this time with updated forecasts of load and renewable infeed profiles.

$$J^{\text{MPC}} = \sum_{l=0}^{N-1} \sum_{i_G=1}^3 [q_{i_G}^G(k+l) (P_{e,i_G}^G(k+l))^2] \quad (12)$$

$$+ q^N(k+l) P_g^G(k+l)] \quad (13)$$

$$+ c_\varepsilon \sum_{l=0}^{N-1} \sum_{i_E \in \Omega_E} (\varepsilon_{i_E}(k+l))^2 \quad (14)$$

$$+ c_{\text{Sched}} \sum_{l=0}^{N-1} \sum_{\mathbf{P}^G} (\mathbf{P}^{G,\text{Sched}}(k+l) - \mathbf{P}^{G,\text{MPC}}(k+l))^2 \quad (15)$$

The optimal values for the generation units are stored in $\mathbf{P}^{G,\text{MPC}} = [P_{e,i_G}^{G,\text{MPC}} \quad P_{g,i_G}^{G,\text{MPC}}]$. Compared with the objective of the pre-scheduler, the MPC controller in addition minimizes deviations from predefined settings of the pre-scheduler, (15). This term represents additional costs for deviations from day-ahead planning, weighted with c_{Sched} . These deviations can either be compensated by buying balancing energy or by adjusting fast backup generators. However, the goal of the MPC controller is to compensate most of these deviations by changing the settings of the storage devices.

Application to System: Finally, the control settings are implemented to the system. Thereby, control variables as defined in (6) are fixed and a power flow calculation is performed. The system has the exact load and renewable infeed profiles which leads again to deviations within the needed supply energy.

$$J^{\text{SYS}} = c_{\varepsilon} \sum_{i_E \in \Omega_E} (\varepsilon_{i_E}(k))^2 \quad (16)$$

$$+ c_E \sum_{i_E \in \Omega_E} (\mathbf{E}_{i_E}^{\text{MPC}}(k) - \mathbf{E}_{i_E}^{\text{SYS}}(k))^2 \quad (17)$$

$$+ c_{\text{MPC}} \sum_{\mathbf{u}} (\mathbf{u}^{\text{MPC}}(k) - \mathbf{u}^{\text{SYS}}(k))^2 \quad (18)$$

If storages are not able to compensate for all forecast errors, i.e., if the system becomes infeasible, control variables are not fixed anymore but are allowed to deviate from the settings defined by the MPC controller. In this case, an additional term (18) is added to the objective function. Any deviation from the predefined MPC settings is penalized by weighting factor c_{MPC} . This term represents costs for spinning reserves or balancing energy. If these reserves are still not enough to bring the system to a feasible operation state, load shedding schemes ought to be applied.

For all three optimization problems, equality constraints are defined by all power flow equations of the electricity and gas networks as well as by the hub equations and storage difference equations. Inequality constraints comprise limits on voltage magnitudes, pressures, changes in compressor settings, dispatch factors, power limitations on hub inputs and limits on storage contents and storage flows (2) - (4).

5 Simulation Results

The proposed control scheme is now applied to the two-hub system depicted in Fig. 4. In a first simulation, operation costs for different storage sizes and different prediction horizon lengths are compared. Secondly, impacts of forecast errors on operation costs are examined. To solve the optimization problems, the solver `snopt` through the Tomlab interface [7] in Matlab (R2008b) is used.

5.1 Simulation Setup

Both hubs have daily profiles of load demands, energy prices and renewable infeeds. In this study, price forecasts are assumed to be perfect, load and renewable infeed forecasts contain uncertainties. Loads and renewable infeed profiles vary more pronounced within the considered time horizon than prices do, therefore, prices are assumed to contain no uncertainties. Electricity prices are modeled on three levels, while gas prices are assumed to be constant during the day. The electric and heat load profiles as depicted in Fig. 5 are standardized profiles of an aggregation of several households. Occurring uncertainties are modeled by superimposing a normal distributed error

signal on the basic load profiles. It is assumed that uncertainties between consecutive time steps are not correlated. However, when modeling a high amount of aggregated households, forecast errors often show a correlation between successive time steps. In [8], a window model is presented, which correlates consecutive forecast errors. Implementing this kind of correlation is subject to further studies.

In a first simulation setup, forecast uncertainties occurring within load profiles are analyzed. In this setup, PV installations are available at both hubs. Figure 6 shows the infeed profiles. These solar curves are assumed to be perfect, i.e. pre-scheduler, MPC controller and the system use the same input curve. The second simulation setup investigates impacts of forecast uncertainties of renewable infeed profiles. For this setup, a wind installations is present at hub H_1 . Figure 6 shows the day-ahead forecast used by the pre-scheduler, R_1^{Sched} , (dotted curve), the updated wind forecast used by the MPC controller, R_1^{MPC} , (dashed curve), and the actual measured wind infeed profile used by the system, R_1^{SYS} , (solid curve)¹. The MPC forecast is generated by superimposing a normal distribution on the actual measured wind infeed profile (10%, $\sigma = 0.05$). The weighting factors $c_{\varepsilon} = 10^3$, $c_{\text{Sched}} = 10^3$, $c_E = 10$ and $c_{\text{MPC}} = 10$ are chosen according to the relative importance of each term.

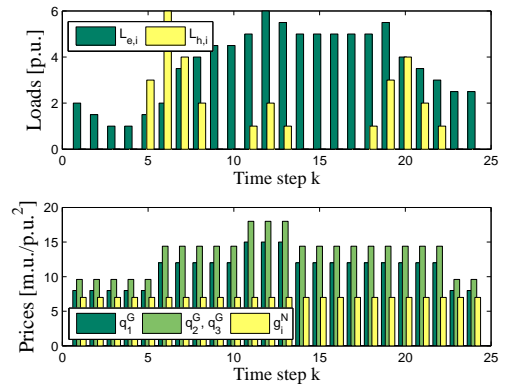


Figure 5: Daily profile for electric $L_{e,i}$ and heat loads $L_{h,i}$ (upper plot), and prices for electricity $q_{i_G}^G$ and natural gas consumption q^N (lower plot).

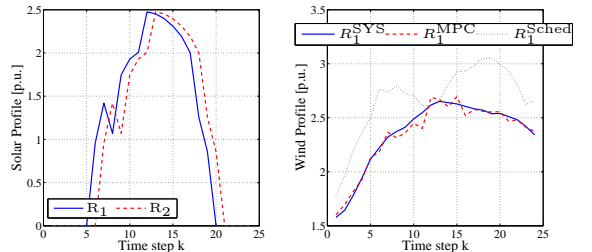


Figure 6: Renewable infeed profiles: Solar measurements (left hand side) and wind forecast profiles (right hand side): exact wind profile (R_1^{SYS}), MPC forecast (R_1^{MPC}), and day-ahead forecast (R_1^{Sched}).

5.2 Impact of Storage Capacity

Combining μ CHPs with heat storage devices permits to supply electric loads via μ CHP, avoiding expensive

¹These renewable infeed curves (scaled) are obtained from solar measurements at Mont Soleil, Switzerland and from wind measurements in Germany.

electricity import during peak times. Battery storages allow for buffering electric energy from renewable energy sources and for releasing it at peak times. In general, storage devices enable to store energy at most beneficial time instants and to release it at instants of optimal usage. For this, not only a sufficient storage capacity is needed, but also the possibility to predict loads and renewable infeeds sufficiently far ahead is necessary. Figure 7 shows the operation costs for different storage sizes and different prediction horizon lengths N . The solid line delineates the costs with basic storage sizes, as they are used for the remaining simulations ($E = [E_{\min}, E^{\max}] = [0.5, 3]$). Increasing the prediction horizon length does not yield essential advantages, since storage capacities are too small. The dashed ($E = [0.5, 5]$) and dotted ($E = [0.5, 8]$) lines show the costs for higher storage capacities. Here, increasing the prediction horizon length enables considerable costs reductions. The further ahead the future prices, loads and renewable infeeds are known, the more efficiently the storage devices can be operated. In this simulation, both storage types have the same capacity. However, only the thermal storage exploits the increased storage capacity. The maximal storage contents are ≈ 7.5 p.u. (per units) for the heat storage and ≈ 7 p.u. for the electricity storage. Consider that these values depend on the chosen load, price and renewable infeed profiles.

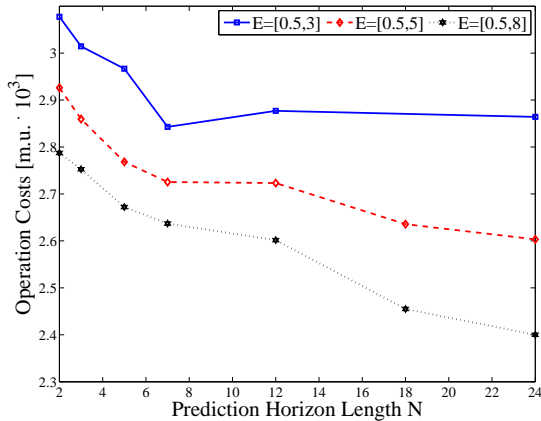


Figure 7: Operation costs for different prediction horizon lengths and different storage capacities.

As can be seen in Fig. 7, high prediction horizon lengths are only advantageous when storage capacities are high enough. However, apart from this operational factor, criteria such as costs of additional storage capacity, availability of reasonable forecasts and computation times need to be considered as well. Beyond that, when forecast errors occur, even larger storages are needed. Basically, the more volatile the disturbances, the less additional storage capacities are needed to compensate the forecast errors, since volatile forecast errors partially balance themselves.

5.3 Impact of Forecast Errors of Load Profiles

Next, the impacts of forecast errors of load profiles on operation costs are examined. For this, the first simulation setup, where both hubs have solar PVs installed,

is used for illustrating the capability of storage devices to balance forecast errors. As mentioned above, randomly distributed disturbances are assumed for the load profiles of electricity and heat. For analyzing stochastic prediction errors, the Monte-Carlo method provides a powerful tool [9]. In order to make significant statements, many simulation runs have to be carried out, resulting in an extensive computational effort. In the following simulations, 100 simulation runs are carried out and therewith the mean value and the standard deviation are calculated. In case of infeasibility, i.e. if storage devices are not able to balance the forecast errors, the system variables are optimized again, allowed to deviate from MPC-settings, (18). Figure 8 shows the distribution of operation costs for a simulation over 24 hours with prediction horizon length $N = 3$. A normal distribution of 15%² is added to each load profile. The histogram can be approximated with a normal distribution (red curve). A mean value of 3056.6 m.u. (monetary units) results which is 1.99% higher than the operation costs without disturbances, 2996.8 m.u. This increase in the mean value is caused by additional costs due to slack variables when storage devices are passing their optimal operational limits as defined in (14). The standard deviation is 38.19 m.u., corresponding to 1.27% of the mean value. Thus, deviations of 15% within the load forecasts can be reduced to 2.54% ($2 \cdot \sigma$) deviation within operation costs. This shows that most of the deviations within load profiles can be compensated by means of storage devices without increasing system operation costs significantly. Table 1 shows mean values and deviations within operation costs for different sizes of forecast errors. The mean values are indicated as percentage increase compared with operation costs without disturbances. Deviations within operation costs, corresponding to two standard deviations, are specified with respect to the according mean values. In general, mean values and standard deviations increase with increasing disturbances.

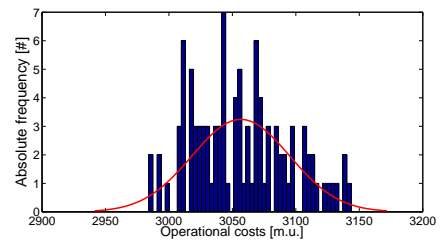


Figure 8: Distribution of operation costs for 15% forecast error.

Forecast error	5%	10%	15%
Increase mean	0.29%	1.16%	1.99%
Deviation ($2 \cdot \sigma$)	1.02%	2.02%	2.54%

Table 1: Mean values and standard deviations for different forecast errors.

Storage devices of higher capacities enable better balancing of forecast errors. Mean values and standard deviations increase less. Note that in this simulation, the pre-scheduler layer has been neglected. When modeling forecast uncertainties with normal distributions, the MPC controller has not more accurate forecasts than the pre-

²96% of all cases lie within 15% deviation of the original value, corresponding to a standard deviation of $\sigma = 0.075$.

scheduler (when assuming the same size of forecast error). Regarding appropriateness, the control settings of the pre-scheduler will be similar to those of the MPC controller, therefore the pre-scheduler can be neglected.

5.4 Impact of Forecast Errors of Renewable Infeed

Now, the second system setup with wind infeed as renewable energy source is considered. At Hub H_1 a wind installation with infeed forecasts as shown in Fig. 6 is installed. Here, the MPC controller has more accurate forecasts than the day-ahead planner. Hence, the pre-scheduler cannot be neglected in this simulation.

Firstly, the pre-scheduler calculates the settings of the generation units, i.e. three generators and gas import, based on the day-ahead forecasts (Fig. 6, dotted curve). Then, the MPC controller updates these setting during the day using updated wind forecasts (Fig. 6, dashed curve). The MPC controller tries to determine settings which deviate as least as possible from day-ahead schedules (15). Figure 9 shows the settings of all three generators of the pre-scheduler (solid curves) and of the MPC controller (dashed curves). Since actual wind infeed is lower than assumed the day-ahead, more electricity has to be generated than planned. All generators slightly increase their production. Since deviations from $P^{G,Sched}$ get penalized, electric storage devices are used to balance the forecast errors as much as possible. Figure 10 shows the storage contents defined by the day-ahead planner (solid curves) and updated by the MPC controller (dashed curves). As can be seen, storage contents are always operated at their lower boundaries to support the underestimated planning of electricity generation.

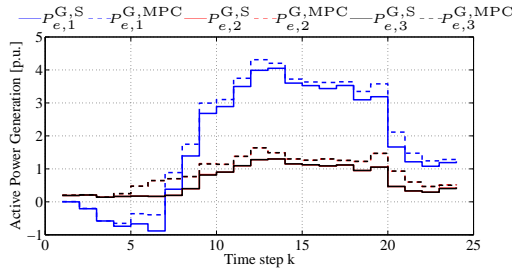


Figure 9: Active power generation of all three generators: settings of day-ahead planner (solid curves) and MPC controller (dashed curves).

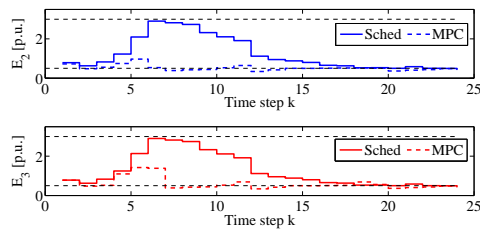


Figure 10: Electric storage devices of both hubs: storage contents defined by the pre-scheduler (solid curves) and by the MPC controller (dashed curves).

Note, that within the first 7 hours, wind infeed exceeds system demand and storage capacities. The surplus power is fed back to the system $P_{e,1}^G < 0$. Alternatively, wind infeed could be modeled as control variable, trying to run it at its maximum but having the possibility to curtail it in cases where the system cannot absorb it anymore.

6 Conclusion and Outlook

We have presented the application of model predictive control to multi-carrier energy systems including storage devices, renewable infeeds and forecast uncertainties. It has been shown that when operating storage devices with a predictive control approach, major part of the disturbances can be compensated by storage devices located close to locations where the uncertainties arise. Therewith, adjustments of fast acting backup generators or penalties for balancing energy can be reduced. Moreover, we have shown that high prediction horizon lengths are only advantageous when storage capacities are high enough. By implementing the MPC controller between the layer of day-ahead planning and the system layer, operation costs are reduced by accounting on future events and taking respective measures early enough, such as storing energy before peak times, changing the settings of a slow acting power plant, or starting up an additional power plant.

Future research includes the implementation of more sophisticated models regarding forecast uncertainties for renewable infeed profiles and the correlation between successive forecast errors. Furthermore, renewable infeed and system load could be implemented as control variables, in order to adapt renewable infeed to system load and for enabling the implementation of load-shedding schemes, respectively. In addition, ramp rates of generation units should be taken into account.

Acknowledgments

This research was supported by the project “Vision of Future Energy Networks” (VoFEN) of ABB, Alstom Grid (formerly Areva T&D), Siemens, and the Swiss Federal Office of Energy.

REFERENCES

- [1] M. Black and G. Strbac. Value of storage in providing balancing services for electricity generation systems with high wind penetration. *Journal of Power Sources*, 162(2):949–953, 2006.
- [2] G. Koeppl and M. Korpås. Using storage devices for compensating uncertainties caused by non-dispatchable generators. Presented at the *9th International Conference on Probabilistic Methods Applied to Power Systems*, Stockholm, Sweden, 2006.
- [3] M. Geidl and G. Andersson. Optimal power flow of multiple energy carriers. *IEEE Transactions on Power Systems*, 22(1):145–155, 2007.
- [4] P. Kundur. *Power System Stability and Control*. McGraw-Hill, New York, New York, 1994.
- [5] M. Arnold, R. R. Negenborn, G. Andersson, and B. De Schutter. Model-based predictive control applied to multi-carrier energy systems. Presented at the *IEEE PES General Meeting 2009*, Calgary, Canada, 2009.
- [6] J. M. Maciejowski. *Predictive Control with Constraints*. Prentice Hall, Harlow, England, 2002.
- [7] P. E. Gill, W. Murray, and M. A. Saunders. SNOPT: An SQP algorithm for large-scale constrained optimization. *SIAM Journal on Optimisation*, 12(4):979–1006, 2002.
- [8] M. A. Ortega-Vazquez and D. S. Kirschen. Economic impact assessment of load forecast errors considering the cost of interruptions. Presented at the *IEEE PES General Meeting 2006*, Montreal, Canada, 2006.
- [9] P. Glasserman. *Monte Carlo methods in financial engineering*. Springer-Verlag New York, Inc., 2004.